Int. J. Appl. Math. Comput. Sci., 2023, Vol. 33, No. 2, 197–205
DOI: 10.34768/amcs-2023-0015

MULTI–SYMPTOM MEASUREMENT BASED FAULT DETECTION OF THE PEM FUEL CELL SYSTEM

ADAM POLAK [a,*], MARCIN KLUCZYK [a]

[a]Faculty of Mechanical and Electrical Engineering
Polish Naval Academy
ul. Śmidowicza 69, 81-127 Gdynia, Poland
e-mail: {a.polak,m.kluczyk}@amw.gdynia.pl

The proper functioning of the fuel cell system depends on the proper operation of all its subsystems. One of the key subsystems is the oxidant supply system, which is responsible for supplying oxygen for the electrochemical reaction taking place in the cell. It also transports the reaction products, i.e., water, outside the fuel cell stack, and in some cases removes excess heat generated in the stack. Changes in the technical condition of machine individual elements always result in changes in operating or residual parameters; however, it is necessary to select appropriate diagnostic methods to be able to use these changes to assess the machine's technical condition. This article presents the results of research focused on assessing the possibilities of diagnosing the oxidant supply subsystem, in particular, too low an oxidant flow leading to oxygen starvation and cathode flooding, based on the analysis of the voltage occurring in individual cells of the stack as well as on the basis of vibration and acoustic emission (AE) measurements. The presented results show that the faulty operation of that system can be indicated either through electrical and vibroacoustic/acoustic emission measurements.

Keywords: PEM fuel cells, failure detection, oxygen starvation, cell flooding, acoustic emission, vibrations.

1. Introduction

Fuel cells (FCs), as a result of a controlled electrochemical reaction taking place on the electrodes of the cell, convert the chemical energy stored in the fuel into electricity. Thanks to the appropriate cell construction, the energy released during the reduction and oxidation reactions can be used to perform external electrical work (Barbir, 2005). One of the most intensively developed fuel cell technologies is the fuel cell with a polymer proton exchange membrane (PEM FC), in which the fuel is pure hydrogen and the oxidant is oxygen, which can come from the atmospheric air, and the reaction product is electricity, heat and water. Thus, such an energy converter does not emit to the environment neither hazardous substances nor greenhouse gases. Among other technologies of fuel cells, they are also distinguished by a relatively low operating temperature, usually in the range of 60–80°C, which in turn allows quick start and stop of the entire system. These cells also do not contain environmentally harmful materials and most of them are recycled. In addition, while maintaining the appropriate purity of the reaction gases, they are distinguished by a relatively long service life of up to 80,000 hours (Ogawa, 2020). The main disadvantages of PEM fuel cells include a relatively expensive catalyst with platinum in its construction and difficult operation at negative temperatures due to the need to moisten the ion-conducting membrane. Moreover, they are particularly sensitive to contamination, especially sulfur compounds (Fox and Colon-Mercado, 2011) and carbon monoxide (van Biert *et al.*, 2016), which irreversibly damage the membrane and catalyst layer.

The proper operation of a fuel cell power system depends on many factors. The basic requirement is to supply the fuel cell stack with the reactants at a rate resulting from the reaction speed taking place therein and to discharge the products of this reaction. Mainly it is water and the reaction heat generated inside the stack. Additional requirements relate to maintaining the stack's operating parameters in specific ranges, i.e., the stack temperature, moistening of the membrane, pressure of reaction gases, etc. A fundamental problem in the operation of fuel cells is the supply of the required

*Corresponding author

amount of reagents to maintain the rate of reduction and oxidation reactions at the level resulting from the electric current drowned from the cell. Reagent deficits during stack operation are significantly detrimental to fuel cells, and basically for this reason health-aware fault tolerant control methods, which have recently gained popularity (Lipiec *et al*., 2022), cannot be directly implemented in fuel cell systems in terms of reactant flow control. A decreased reagent flow contributes to accelerated degradation of active elements as well as may lead to irreversible damage to the cell. The most common are membrane perforation, migration of catalyst particles to the membrane, re-formation of hydrogen molecules on the cathode side and then direct reaction with the oxygen available in the cathode compartment, and formation of the so-called "hot spikes" (Barbir, 2005). Another important phenomenon that may occur with an insufficient oxidant flow through the cathode section of the fuel cell stack is water vapor condensation. Insufficient ventilation of the cathode compartment can lead to blockage of a part of the active cathode surface of a single cell as well as complete blockage of the oxidant flow by several cells in the stack, leading to oxygen starvation and cessation of the reaction in these cells.

The problem of malfunction diagnosis consists of a few stages detection, localization of faults and identification or analysis to provide the essential information of fault determination, i.e., type, magnitude and causes (Benmouna *et al*., 2017). The main criterion of classifying diagnostic methods might be model based methods and non-model based methods. The first type is considered an analytical approach that requires a comprehensive understanding of the cell and its inner phenomena. A series of key relations of the different natures (electrochemical, thermodynamic, thermal, electrical and fluidic) are necessary to develop this model (Benmouna *et al*., 2017). The objective of non-model methods is to obtain fault information based on heuristic knowledge or signal processing, or a combination of both (Benmouna *et al*., 2017). Diagnostic methods belonging to both groups are currently being studied in terms of implementation in fuel cells (FCs) diagnostics (Hissel and Péra, 2016; Pivac *et al*., 2017; Najafi *et al*., 2020). Acoustic emission (AE) analysis is one of possible methods of FC diagnostic.

The essential tool for an on-line assessment of the proper operation of the fuel cell system is the observation of the voltages on the cells of the stack. Abnormalities in the operation of the fuel cell system can be observed at the voltages of either individual cells or at the voltage of the entire stack. Continuous observation and analysis of these voltages enable relatively quick detection of abnormalities in the operation of the fuel cell system and allow the control unit to perform proper actions to prevent stack degradation or system damage.

The AE measurement technique is based on generation of acoustic waves by fast propagating micro-failure processes or other sources (He *et al*., 2021). The AE process occurs when the material undergoes irreversible changes in its internal structure. The reason for such changes may be the forces occurring when the material is loaded, but also, for example, the corrosion process or temperature changes. Highly sensitive, usually passive piezoelectric transducers detect these waves by dynamic surface motion on a sub-nanometer scale and convert them into an electric signal. The measurement frequency range is usually about 50 kHz to 1 MHz. Lower frequencies are often associated with extraneous noise sources or resonance effects of the transducer case and they should be identified before the analysis. Higher frequencies are excessively damped especially in non-metal materials, and these high-frequency parts of waves are carried to a distance no longer than a few centimeters from the source location (Bohse, 2004). However, if they are transferred to metal elements, they might be detected at a longer distance. Acoustic methods are becoming a very useful tool in the study of processes occurring inside electrochemical power systems and have the advantage of relatively low cost and non-invasive operation (Bethapudi *et al*., 2019).

A few works connected with acoustic emission monitoring have been implemented, but they are mainly connected with measurements of a single cell (Legros *et al*., 2010). Also, a lot of methods dedicated especially to fuel cells might be found in the works of Wu *et al*. (2008), Benmouna *et al*. (2017), Wang *et al*. (2011), or He *et al*. (2021)

The sensitivity of an acoustic emission system is often limited by the amount of background noise nearby. Noise in AE testing refers to any undesirable signals detected by the sensors. The source of EA phenomena may also be the devices and structures surrounding the FC. Elastic waves propagate through the supporting structure to the AE sensor mounted on the diagnosed device. Therefore, it is important to determine the background noise level when the diagnosed device is not working. The most popular solution used to compensate the effects of background noise is setting the proper value of the recording threshold (Legros *et al.*, 2010; 2023). This threshold is the limit beyond which the acquisition system will take the corresponding burst into account and record it, allowing further data treatment to be performed later. A threshold value of 40 d_{BAE} was set. This was done after initial measurements, to prevent the AE signals from recording background noise.

In this paper we show that both measurements and analysis of cell voltages and AE measurements can indicate a problem regarding oxygen supply in the PEM fuel cell system.

Table 1. Parameters of the PEM fuel cells stack.

Quantity	Value	Unit
Number of cells	68	–
Cell active area	200	cm^3
Nominal power	6000	W
Maximum power	8000	W
Maximum voltage	68	V
Minimum voltage	32	V
Maximum current	250	A
Nominal operating temperature	65	°C
Anode stoichiometry	1.25	–
Cathode stoichiometry	2	–
Reactants relative humidity	99	% RH
Anode to cathode pressure diff.	<0.3	bar
Reactants purity	>99.99	%

2. Materials and methods

The experiment was performed on a technology demonstrator of emergency power supply for a submarine in which the main energy source is a PEM fuel cell stack (see Fig. 1), whose main parameters are presented in Table 1. The system operates with pure hydrogen and pure oxygen, and nitrogen is used to flush the system before and after operation.

Other essential components of the fuel cell system are hydrogen, oxygen and nitrogen pressure tanks, a valves and reducers block, flow regulators, diaphragm reactor gas humidifiers, steam traps, a hydrogen recirculation pump, heat exchangers, pressure and temperature sensors, and a supervisory control and measurement system. The structure of the system is presented in Fig. 2.

The experimental design assumed introduction of a disturbance to the operation of the fuel cell system consisting in the reduction of the cathode stoichiometry. Before starting the experiment, the system was brought to the nominal operating temperature, and then the fuel cell stack was operating for several minutes under a constant load and a constant high cathode stoichiometry equal to 1.5. During the experiment, the stack load, its temperature, and the pressure of reaction gases were kept constant. Measurements were started after the stack operation parameters had stabilized. In the initial stage, the cathode stoichiometry was maintained at the level of 1.5, then, after a few seconds, it was reduced to the level of 1.0. Based on our previous experience it is assumed that this reduction in the oxygen flow leads to observable voltage changes (Polak, 2017). Moreover, if the voltages on individual cells of the stack do not drop below a minimum assumed level, it is relatively safe for the fuel cells stack in case of short term operation. After approximately 300 s from the start of the measurement, the cathode stoichiometry was restored to the initial

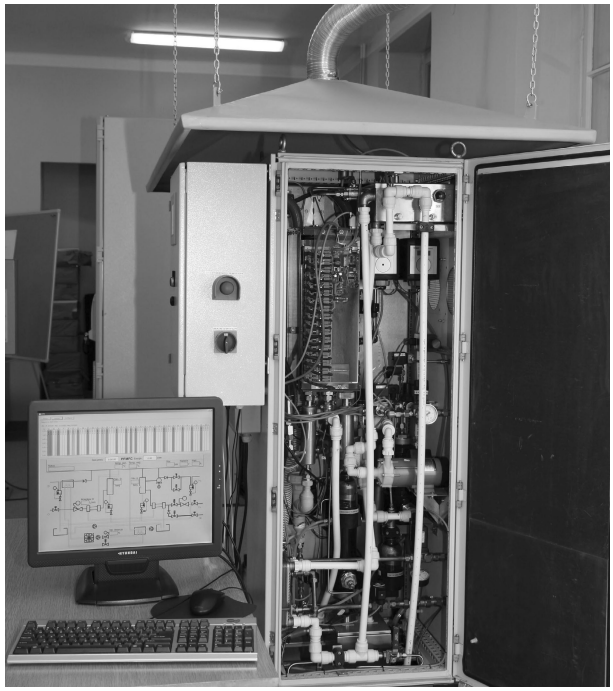

Fig. 1. 6 kW PEM fuel cell system.

value equal to 1.5, and the experiment was continued for approximately 820 seconds counting from the start of the measurements. During the experiment, measurements of the basic operating parameters of the system were made, i.e., pressure of reaction gases, the inlet and outlet cooling water temperature, oxygen flow, and electrical parameters such as the current and voltage of the stack and the voltages of all stack cells. The measurements of the above values were made with the use of the built-in monitoring and control unit of the system at the frequency of 5 Hz.

Acoustic emission and vibrations were measured using additional measuring systems. The AE system used during the experiments has an input range at the level of 100 d_{BAE} with a sampling rate of 2 MHz. It can be used with AE sensors operating in a frequency from 20 kHz to 500 kHz. It was connected with a VS150 L AE sensor, which is a passive piezoelectric AE sensor. Its frequency response is characterized by a peak at 150 kHz, where it exhibits a resonance. It is suitable for almost all AE applications. The sensor has a full metal housing that makes it especially well suited for adhesively mounting it to a test object. In this respect, it is appropriate for inspecting objects that have no ferro-magnetic surface such as composites. The sensor has a mass of 26 g and a frequency range from 100 to 450 kHz. A general view of the sensor and its frequency characteristic is presented in Fig. 3. A measurement of an AE signal is triggered when the AE signal exceeds a certain, user defined, detection threshold. During the measurements a threshold equal to 40 d_{BAE} was set. An AE signal that exceeds the

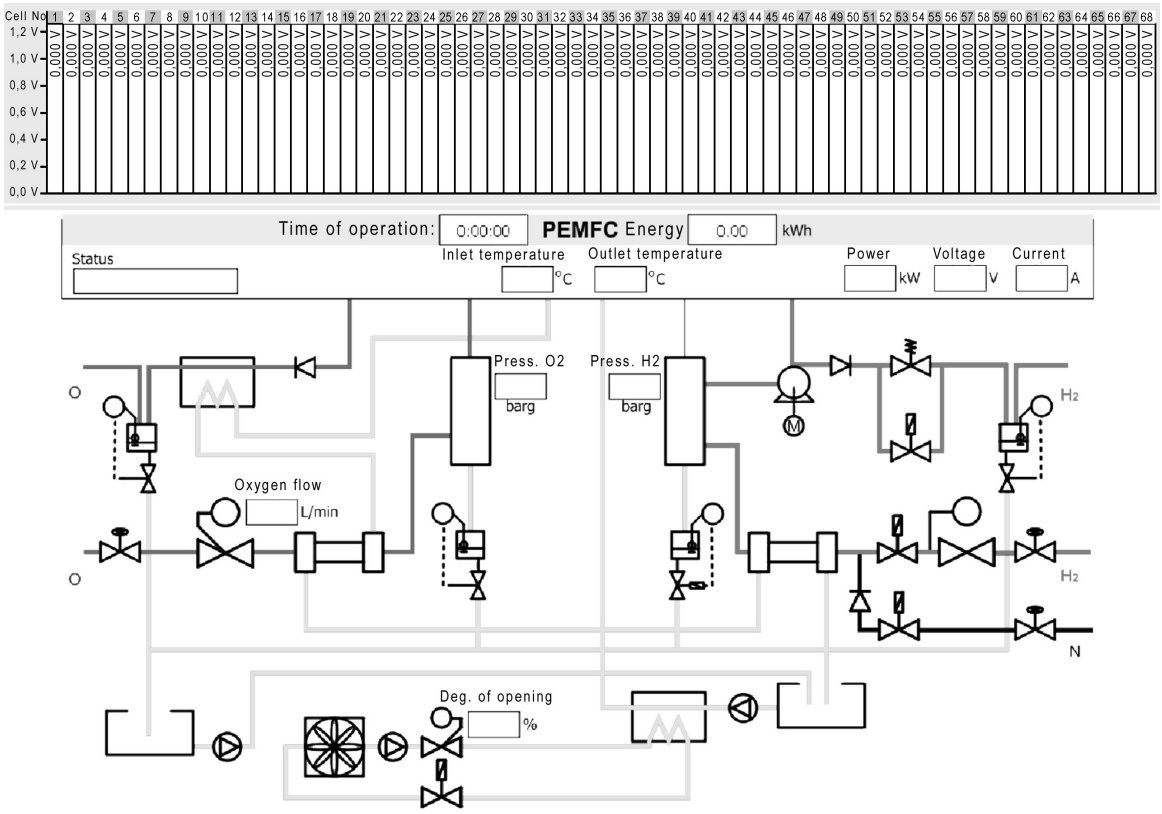

Fig. 2. Diagram of the fuel cell system.

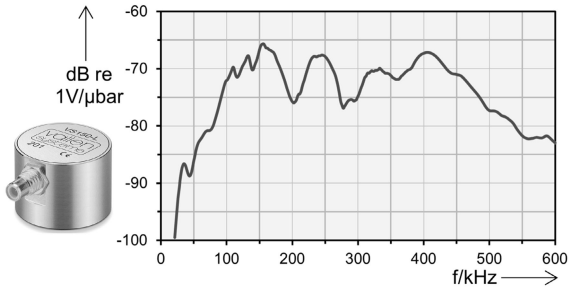

Fig. 3. Vallen VS150 L AE sensor and its characteristic.

detection threshold is called a detected burst signal or hit. The next important parameter during AE measurements is the band pass filter, which was set to 100–500 kHz. Additionally, the duration discrimination time was set as 800 µs. The sensor location during measurements is presented in Fig. 4.

During the experiment also vibration accelerations were recorded. The sampling frequency was set to 131072 Hz, and the analyzed frequency span was 51.2 kHz. The accelerometer was located next to the AE sensor (Fig. 3). A linear characteristic with an error of no more than 10% for the sensor applied is ensured in the frequency range of 10 Hz to 10,000 Hz. We deliberately took measurements at much higher frequencies in order to determine the suitability of a traditional vibration measurement system for fuel cell diagnostics. For the AE analysis, a Vallen Visual AE software was used, while the vibration signals analysis was performed with Pulse Reflex.

3. Experimental results

The analysis of the voltages acquired during the experiment was performed in the Matlab environment. The analysis of the AE measurements and the vibration acceleration measurements was performed with dedicated software.

3.1. Analysis of the voltages on the cells of the stack. In the first step, a direct comparison of the voltage distribution on the stack cells for the four time moments marked in Fig. 5, showing the changes in the cathode stoichiometry, was made. This is respectively the beginning of the experiment, when the cathode stoichiometry was 1.5 (a), half the duration of the stoichiometry decreased to 1 (b), right before the stoichiometry was increased (c), and when the stoichiometry was restored to 1.5 (d).

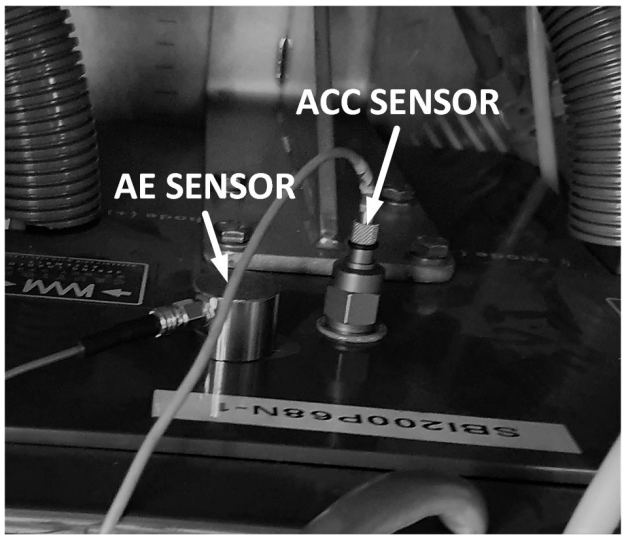

Fig. 4. Localization of the AE sensor and accelerometer on top of the PEM FC stack.

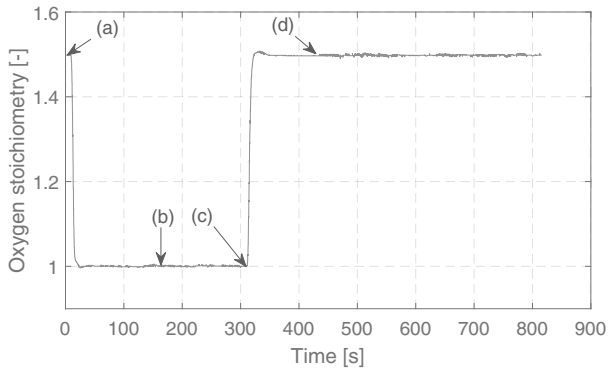

Fig. 5. Oxygen stoichiometry changes during the experiment.

Figure 6 shows graphs of voltage values on all cells of the stack for selected moments.

In all plots, it can be seen that those at high numbered cells are higher than the voltages at lower numbered cells. This is not due to a system malfunctioning, but to the construction of the stack, where high numbered cells are at the oxygen inlet of the stack and lower numbered cells are at the oxygen outlet of the stack. Such a construction causes this distribution of cell voltages due to differences in oxygen concentration across the stack. Moreover, it can also be observed that the introduction of the disturbance in the form of decreased cathode stoichiometry makes the voltage dispersion on the cells in the stack go up over time. This phenomenon can be a good diagnostic symptom to indicate system malfunctions. Moreover, it can be seen that, as the disturbance continues, the voltages on some cells differ significantly from those on the other cells (Fig. 6(c)). This may suggest that these cells suffer the more severe consequences of reduced stoichiometry, i.e., they are experiencing more intense water vapor condensation and greater oxygen starvation.

In the next step, for each measurement point resulting from the frequency of measurements, the average value of the voltages in the stack v_m and the voltage range in the stack v_r (the difference between the maximum and minimum voltage occurring on individual cells of the stack) were determined in accordance with

$$v_r = v_{\max} - v_{\min}, \tag{1}$$

$$v_m = \frac{1}{68}\sum_{i=1}^{68} v_i. \tag{2}$$

Moreover, the variance v_{var} and the standard deviation σ_v of the stack voltages were calculated as

$$v_{\text{var}} = \frac{1}{68}\sum_{i=1}^{68}(v_i - v_m)^2, \tag{3}$$

$$\sigma_v = \sqrt{\frac{1}{68}\sum_{i=1}^{68}(v_i - v_m)^2}. \tag{4}$$

Then, the calculations of relative changes in the values of these quantities were performed, where the reference value was that obtained for the time $t = 0$

$$\text{CHANGE}(v_r) = 100\frac{v_{r,t_j}}{v_{r,t_0}} - 100, \tag{5}$$

$$\text{CHANGE}(v_{\text{var}}) = 100\frac{v_{\text{var},t_j}}{v_{\text{var},t_0}} - 100, \tag{6}$$

$$\text{CHANGE}(\sigma_v) = 100\frac{\sigma_{v,t_j}}{\sigma_{v,t_0}} - 100. \tag{7}$$

The obtained results of changes in the relative value of the range, variance and standard deviation over the entire experiment are shown in Fig. 7. The dotted rectangle depicts the area which is zoomed and presented in Fig. 8.

The analysis of the results presented in Fig. 7 shows an increase in all selected indicators along with the duration of the disturbance introduced. The smallest initial change can be seen in the course of the voltage range. On the enlargement of the fragment of the graph presented in Fig. 8, it can be seen that relatively significant changes are only observable after around 1000 s of the experiment. The value of the stack voltage range doubled at approximately 2000 s from the start of the experiment and reached its maximum value at the end of the period of lowered cathode stoichiometry, where the range increased by almost 300% from the beginning of the experiment. The other two indicators, i.e., variance and standard deviation, started to increase much earlier after lowering the cathode stoichiometry.

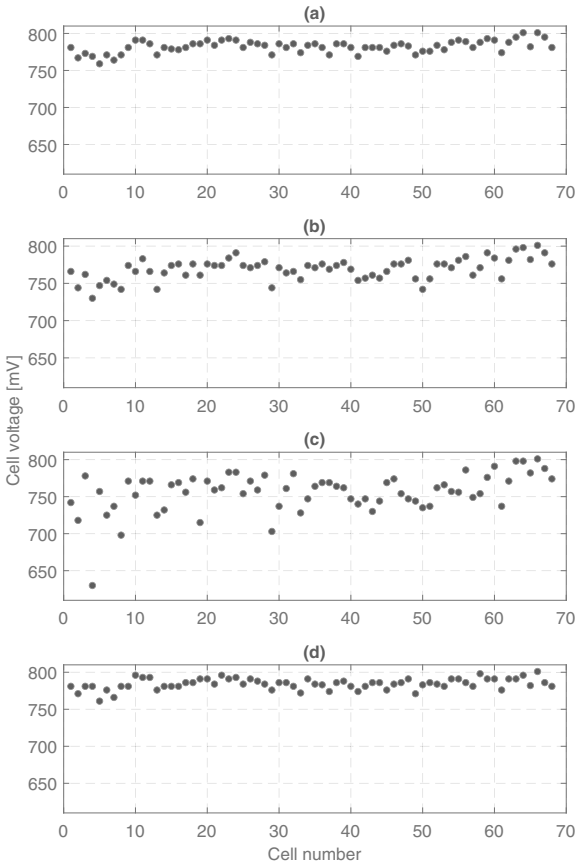

Fig. 6. Voltage dispersion change across the stack during the experiment: at the beginning of the experiment oxygen stoichiometry equals 1.5 (a), in the middle of the introduced fault oxygen stoichiometry equals 1.0 (b), at the end of the introduced fault oxygen stoichiometry equals 1.0 (c), at the end of the experiment stoichiometry recovers to 1.5 (d).

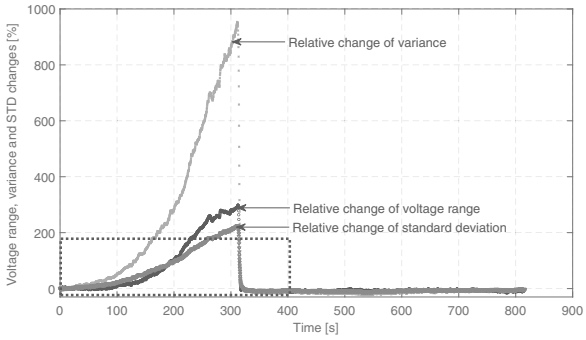

Fig. 7. Voltage range, variance and standard deviation relative value changes during the experiment.

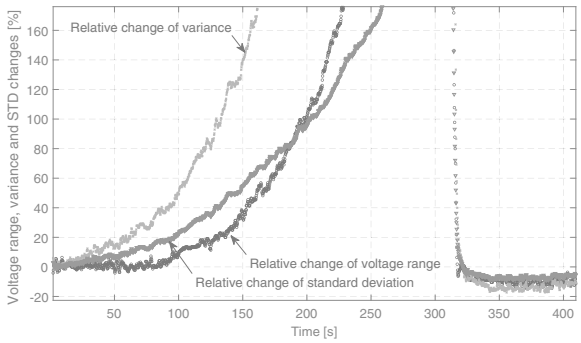

Fig. 8. Zoomed area of voltage range, variance and standard deviation relative value changes during the experiment.

In Fig. 8 it can be seen that both these indicators begin to increase almost immediately after reducing the oxygen flow. These indices increased by about 20% after approximately 50 and 100 s, respectively. The variance doubled around 130 s after the disturbance was introduced, and the standard deviation doubled after around 200 s. The maximum values, i.e., 960% of the initial value of the variance and 215% of the initial value of the standard deviation, were reached at the end of the period in which the reduced cathode stoichiometry was maintained (approximately 315 s of the measurement). It can also be noticed that, immediately after the initial value of the stoichiometry was restored, the indices decreased very quickly, reaching values even lower than those observed at the beginning of the experiment.

3.2. AE and vibroacoustic analysis. The data collected during the experiment were analyzed using visual acoustic emission software. The AE signal was analyzed during three steps. First of all, the rise time of hits as a time function was plotted (Fig. 9). The rise time is the time measured from the moment when the AE hit exceeds the threshold limit until the maximum amplitude values are reached. Secondly, the burst signal energy in the time domain was analyzed (Fig. 10). The last step was the analysis of the hit duration calculated as the time from exceeding the threshold value to the time of reaching the value below this determined value (Fig. 11). Analysis of Figs. 9–11 leads to the conclusion that all presented acoustic emission hits parameters significantly increase their value during the introduced disturbance in the oxygen flow (around 200 seconds from the measurement start). Growth takes place in a short time, and recovery to the baseline state from before the failure takes much longer; however, the highest values disappeared quite fast. What is more, all parameters are strongly connected. Careful analysis leads to the conclusion that the energy, the rise time and the duration of each AE hit which

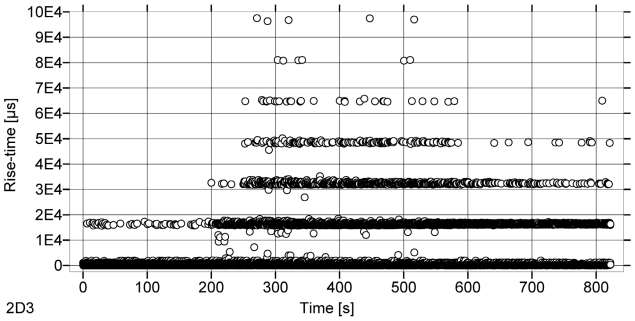

Fig. 9. Rise time of hits during PEM FC stack fault simulation.

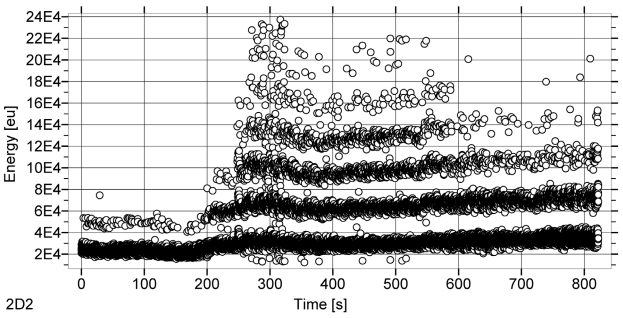

Fig. 10. Hits energy during PEM FC stack fault simulation.

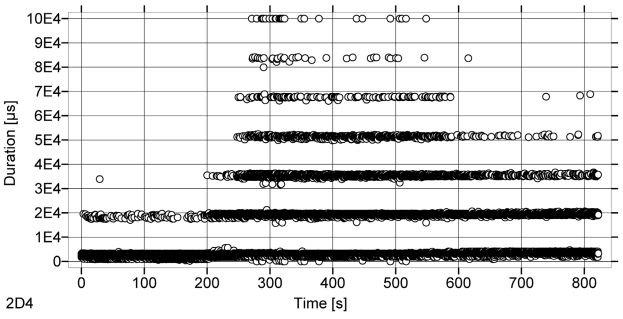

Fig. 11. AE burst signals duration during PEM FC stack fault simulation.

occur after the introduction of the disturbance are strictly correlated with each other.

The analysis of the registered vibration accelerations was divided into two stages. In the first one, the broadband STFT analysis was performed, ensuring the resolution in the frequency domain at the level of 8 Hz, which at the analyzed 51.2 kHz band allowed obtaining 6400 lines in the spectrum presented in Fig. 12. There is a noticeable increase in the value of vibration amplitudes in a wide band at the time when the failure was introduced. In this case, the analyzed signal was not subjected to any filtration process.

The second stage of the vibration data analysis was to determine the average values of vibration accelerations in one-second intervals. Such an analysis was carried out for three frequency ranges, i.e., the useful range of the sensor, 10–10000 Hz, and two ranges where the linearity of the sensor signal is not guaranteed, i.e. 10000–20000 Hz and 20000–30000 Hz. The obtained vibration results are shown in Fig. 13. Significant changes in the value of vibration accelerations caused by the introduced disturbance in the oxygen flow are clearly visible only in the frequency ranges in which the sensor should not be used.

4. Discussion

Despite the long-term operation of a system with the disturbance, consisting in reducing the cathode stoichiometry of the stack to the value of 1, no sudden cell reversal occurred at any of the cells, as was shown by Taniguchi *et al*. (2008). However, in this experiment the authors reduced the stoichiometry down to the level of 0.83. During the experiment, no voltage oscillations were observed on the cells as shown by Niroumand *et al*. (2011). On the other hand, slow changes consisting in increasing the dispersion of voltages in the stack were observed. Important for this observation is also the fact that for a certain period of time, in which there were no significant changes in the voltage range, other indicators, i.e., variance and standard deviation, already indicated an increasing dispersion of the voltage values in the stack. After maintaining the reduced oxygen flow for a longer time, it was also noticed that the voltages at some cells differ significantly from the other voltages. This may indicate the fact that the smallest amounts of oxygen were supplied to these cells, which in consequence could lead to local flooding of the cell and oxygen starvation.

The disturbance introduced in the flow of oxygen in the stack caused that at least one cell was operating in abnormal conditions, which resulted in increased stresses in the membrane (Matsuura *et al*., 2013). These in turn resulted in high-frequency acoustic emission events. Despite the fact that the sensors used during the tests were not mounted directly on the cell on which the simulated damages were made, but on the casing of the entire stack, the signal transmittance was so high that it was possible to register the signals using both the sensor for measuring accelerations and the sensor for measuring acoustic emission phenomena. It should be emphasized here that we consciously used a typical accelerometer sensor ensuring linear characteristics of the measured signal in the frequency range typical for most normative documents, i.e., 10–1000 Hz. As it turns out, in this respect, the energy of the registered vibration phenomena is so low that small and difficult to detect changes in the signal occur in the averaged time

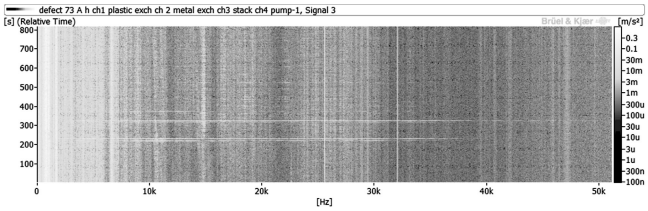

Fig. 12. Vibration acceleration STFT spectrum.

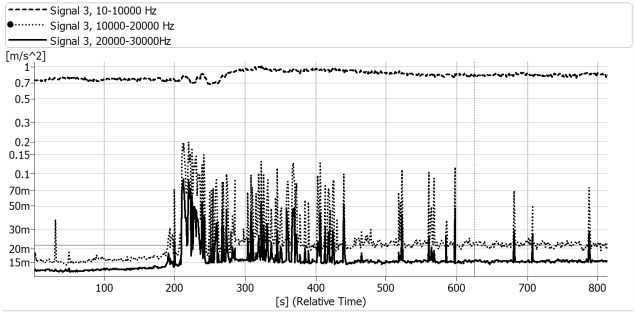

Fig. 13. Averaged waveforms for one-second intervals.

course. On the other hand, clearly noticeable changes occur in relation to phenomena with frequencies higher than typical applications of the sensor used.

5. Conclusions

This study attempted to determine the possibility of using cell voltage analysis as well as vibration measurements and AE for the needs of diagnostics of a failure of the PEM FC stack resulting from inappropriate oxygen management. The presented research showed that the measurements of the voltage on the stack cells and their on-line statistical analysis can be used to diagnose abnormalities in the stack's operation, and in particular, irregularities in the supply of oxidant to the stack. Determining the variance or the standard deviation of the stack voltages enables faster detection of abnormal stack operation compared with the observation of only absolute changes in the voltages on the cells in the stack. Moreover, it turns out that both methods, AE and vibration measurements, can be used for this purpose, but the method of measuring acoustic emission is more reliable. This is due to the fact that the elastic waves generated in the membrane have frequencies that exceed the measuring range of typical accelerometers. Therefore, it is justified to conduct future measurements in this area only with the use of AE sensors, which are designed to detect high frequency phenomena.

References

Barbir, F. (2005). *PEM Fuel Cell Theory and Practice*, Elsevier/Academic Press, Burlington.

Benmouna, A., Becherif, M., Depernet, D., Gustin, F., Ramadan, H. and Fukuhara, S. (2017). Fault diagnosis methods for proton exchange membrane fuel cell system, *International Journal of Hydrogen Energy* **42**(2): 1534–1543.

Bethapudi, V., Maier, M., Hinds, G., Shearing, P., Brett, D. and Coppens, M.-O. (2019). Acoustic emission as a function of polarisation: Diagnosis of polymer electrolyte fuel cell hydration state, *Electrochemistry Communications* **109**: 106582.

Bohse, J. (2004). Acoustic emission examination of polymer-matrix composites, *Journal of Acoustic Emission* **22**: 208–223.

Fox, E.B. and Colon-Mercado, H.R. (2011). Mass transport limitations in proton exchange membrane fuel cells and electrolyzers, *in* H. Nakajima (Ed.), *Mass Transfer*, IntechOpen, Rijeka, Chapter 13, pp. 305–318, DOI: 10.5772/20349.

He, Y., Li, M., Meng, Z., Chen, S., Huang, S., Hu, Y. and Zou, X. (2021). An overview of acoustic emission inspection and monitoring technology in the key components of renewable energy systems, *Mechanical Systems and Signal Processing* **148**: 107146.

Hissel, D. and Péra, M.-C. (2016). Diagnostic & health management of fuel cell systems: Issues and solutions, *Annual Reviews in Control* **42**: 201–211.

Legros, B., Thivel, P.-X., Bultel, Y., Boinet, M. and Nogueira, R. (2010). Acoustic emission: Towards a real-time diagnosis technique for proton exchange membrane fuel cell operation, *Journal of Power Sources* **195**(24): 8124–8133.

Legros, B.and Thivel, P.-X., Bultel, Y. and Nogueira, R. (2023). PEMFC on line diagnosis via acoustic emission measurements, `https://www.sintef.no/globalassets/project/fc-tools/dokumenter/presentation/4a/thivel.pdf`.

Lipiec, B., Mrugalski, M., Witczak, M. and Stetter, R. (2022). Towards a health-aware fault tolerant control of complex systems: A vehicle fleet case, *International Journal of Applied Mathematics and Computer Science* **32**(4): 619–634, DOI: 10.34768/amcs-2022-0043.

Matsuura, T., Chen, J., Siegel, J.B. and Stefanopoulou, A.G. (2013). Degradation phenomena in PEM fuel cell with dead-ended anode, *International Journal of Hydrogen Energy* **38**(26): 11346–11356.

Najafi, B., Bonomi, P., Casalegno, A., Rinaldi, F. and Baricci, A. (2020). Rapid fault diagnosis of PEM fuel cells through optimal electrochemical impedance spectroscopy tests, *Energies* **13**(14), Paper ID: 3643.

Niroumand, A.M., Mérida, W. and Saif, M. (2011). PEM fuel cell low flow FDI, *Journal of Process Control* **21**(4): 602–612.

Ogawa, M. (2020). Toshiba hydrogen business and fuel cells, `https://www.bdi.fr/wp-content/uploads/2`

020/12/Toshiba-H2-biz-and-FC-Rev0-16dec2020.pdf.

Pivac, I., Radica, G., Barbir, F., Benouioua, D., Harel, F. and Candusso, D. (2017). Diagnostic methods for automotive fuel cell systems, *Technical Report D-1.4*, European Commission, Brussels, https://ec.europa.eu/research/participants/documents/downloadPublic?documentIds=080166e5b77c06fa&appId=PPGMS.

Polak, A. (2017). PEM hydrogen fuel cells—Experimental studies on the effect of oxygen flow rate on the polymer membrane, *Polymer Processing* **176**(2): 123–133, (in Polish).

Taniguchi, A., Akita, T., Yasuda, K. and Miyazaki, Y. (2008). Analysis of degradation in PEMFC caused by cell reversal during air starvation, *International Journal of Hydrogen Energy* **33**(9): 2323–2329.

van Biert, L., Godjevac, M., Visser, K. and Aravind, P. (2016). A review of fuel cell systems for maritime applications, *Journal of Power Sources* **327**: 345–364.

Wang, H., Yuan, X.-Z. and Li, H. (Eds) (2011). *PEM Fuel Cell Diagnostic Tools*, CRC Press, Boca Raton, DOI: 10.1201/b11100.

Wu, J., Zi Yuan, X., Wang, H., Blanco, M., Martin, J.J. and Zhang, J. (2008). Diagnostic tools in PEM fuel cell research. Part II: Physical/chemical methods, *International Journal of Hydrogen Energy* **33**(6): 1747–1757.

Adam Polak received his MS degree from the Faculty of Mechanical and Electrical Engineering of the Polish Naval Academy in Gdynia in 2005. Since 2010 he has been holding a research and teaching position at that faculty, and since 2019 he has been the head of the Department of Ship Electrical Engineering there. In 2019 he obtained his PhD in mechanical engineering. His research activities are related to fuel cell systems and their adaptation to maritime applications. Moreover, he is interested in renewable energy sources and energy harvesting techniques.

Marcin Kluczyk was the first mechanic on board a Polish minesweeper in the years 2007–2011. Since 2011, he has been working at the Polish Naval Academy in Gdynia, where he deals mainly with technical diagnostics of marine devices, with particular emphasis on vibroacoustic diagnostics. In 2018 he obtained his PhD degree in machine construction and operation. He is the author of over 40 publications and a contractor of more than 40 expert opinions in the field of vibration diagnostics.

Received: 8 November 2022
Revised: 2 February 2023
Accepted: 7 February 2023